ChemPubSoc Europe

DOI: 10.1002/chem.201502093

CHEMISTRY A European Journal Full Paper

Chelates

The Influence of the Amide Linkage in the Fe^{III}-Binding Properties of Catechol-Modified Rosamine Derivatives

Carla Queirós,[b] Andreia Leite,[a] Maria G. M. Couto,[a] Luís Cunha-Silva,[b] Giampaolo Barone,[c] Baltazar de Castro,[b] Maria Rangel,[d] André M. N. Silva,*[a] and Ana M. G. Silva*[a]

Abstract: The two new fluorescent ligands **RosCat1** and **RosCat2** contain catechol receptors connected to rosamine platforms through an amide linkage and were synthesized by using microwave-assisted coupling reactions of carboxyl- or amine-substituted rosamines with the corresponding catechol units and subsequent deprotection. **RosCat1** possesses a reverse amide, whereas **RosCat2** has the usual oriented amide bond (HNCO vs. CONH, respectively). The ligands were characterized by means of NMR spectroscopy, mass-spectrometry, and DFT calculations and X-ray crystallography studies for **RosCat1**. The influence of the amide linkage on the photophysical properties of the fluorescent ligands was assessed in different solvents and showed a higher fluorescence quantum yield for **RosCat1**. The coordination chemistry of these ligands with a Fe^{III} center has been rationalized by mass-spectrometric analysis and semiempirical calculations. Octahedral Fe^{III} complexes were obtained by the chelation of three **RosCat1** or **RosCat2** ligands. Interestingly, the unconventional amide connectivity in **RosCat1** imposes the formation of an eight-membered ring on the chelate complex through a "salicylate-type" mode of coordination.

Introduction

Iron is vital for life because it participates in several metabolic processes. It can, however, be toxic and the deregulation of its concentration can cause serious disorders and diseases.[1,2] Therefore, the production of iron chelators for its removal or delivery and probes for concentration sensing in biological samples has been a major goal in the field of medicinal chemistry.

Plants and bacteria use highly effective chelating agents, termed siderophores, to acquire this essential micronutrient.[3] Amongst the different siderophores, catechol-based molecules present the highest selectivity and Fe^{III}-binding affinity.[4] The properties of these iron-binding moieties have been explored by synthetic chemists and many catechol conjugates with various functionalized molecules (e.g., drugs or fluorescent probes) have arisen for wide-ranging applications, including drug delivery, bacterial detection, diagnosis, cancer-cell recognition,[5] and sensing.[6]

Our group is particularly interested in the design of new iron chelators for biological and environmental applications, and over recent years we have developed several new bidentate and hexadentate ligands by using catechol units. Inspired by the structure of enterobactin (Figure 1), the siderophore with the highest known Fe^{III}-binding affinity,[7] we have extensively used the amide linkage to conjugate catecholate units with fluorescent molecules[8,9] or tripodal scaffolds.[10] In fact, amides are a reliable and popular functional group of organic chemistry that convene important properties to compounds, such as high stability, polarity, and conformational diversity.[11]

In **catTHC**, the backbone and amide-linkage domains of enterobactin were replaced by a tripodal backbone containing terminal carboxylate functions and a reverse amide connectivity (Figure 1). Also, an additional CH_2 spacer was introduced between the amide and catechol units. As result, the electronic density of the catecholate ring is more affected by the amide bond in enterobactin than in **catTHC**, a fact that can explain the lower Fe^{III}-affinity constant of **catTHC** relative to enterobactin.[10]

In this context, the bidentate fluorescent probes **Cat1** and **RhodCat** were built by using the same reverse amide connector to conjugate the catechol unit to a fluorescein or

[a] *Dr. A. Leite, M. G. M. Couto, Dr. A. M. N. Silva, Dr. A. M. G. Silva*
UCIBIO-REQUIMTE, Departamento de Química e Bioquímica
Faculdade de Ciências, Universidade do Porto
4169-007 Porto (Portugal)
E-mail: ana.silva@fc.up.pt
andre.silva@fc.up.pt

[b] *C. Queirós, Dr. L. Cunha-Silva, Prof. B. de Castro*
LAQV-REQUIMTE, Departamento de Química e Bioquímica
Faculdade de Ciências, Universidade do Porto
4169-007 Porto (Portugal)

[c] *Prof. G. Barone*
Dipartimento di Scienze e Tecnologie Biologiche
Chimiche e Farmaceutiche (STEBICEF), Università di Palermo
Vialle delle Scienze, Edifício 17, 90128 Palermo (Italy)

[d] *Prof. M. Rangel*
UCIBIO-REQUIMTE
Instituto de Ciências Biomédicas de Abel Salazar
Universidade do Porto, 4050-313 Porto (Portugal)

Supporting information for this article is available on the WWW under http://dx.doi.org/10.1002/chem.201502093.

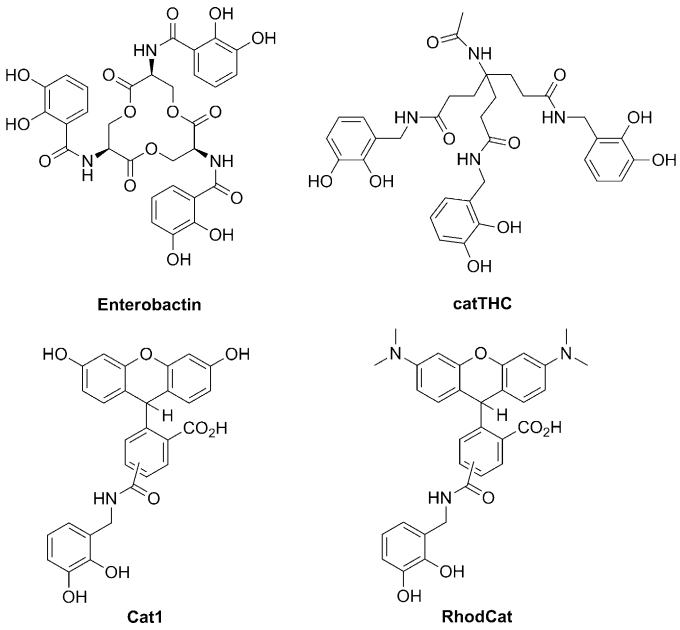

Figure 1. Structures of enterobactin, **catTHC**, **Cat1**, and **RhodCat**.

rhodamine analogue, respectively (Figure 1).[8,9] Both conjugates exhibited similar fluorescence quenching in the presence of Fe^{III} species in aqueous medium.

In the set of molecules designed by our group, a reserve amide linkage was used to bind the catechol unit in contrast to the amide function observed in enterobactin and related catecholate analogues. This reverse linkage has been less explored,[12,13] and little is known about its effects in the coordination of iron ions. Raymond and co-workers have shown that the amide function plays a fundamental role in iron binding by catecholamides, thus allowing for a catecholate and a salicylate coordination mode.[14–16] Furthermore, a significantly different behavior has been reported for both amide configurations.[17,18] Thus, we undertook the task of investigating the effect of amide configuration on the properties of fluorescent catechol conjugates.

Herein, we present the synthesis, characterization, and coordination studies with Fe^{III} ions of a new family of fluorescent bidentate ligands, namely, **RosCat1** and **RosCat2**, containing a catechol-chelating unit connected through an amide linkage to a rosamine platform (Figure 2). This family of fluorescent ligands was designed to study the influence of the amide linkage on the metal-binding properties of the catechol ligands. We chose the rosamine scaffold as the fluorophore because, in contrast to rhodamine derivatives, it lacks a carboxylic group at the *ortho*-position of the phenyl ring and therefore does not generate the nonfluorescent and colorless spirocyclic form. Additionally, rosamines can be easily isolated as a single regioisomer and are less problematic to synthesize and purify.[19] Furthermore, the introduction of substituents that decrease the basicity of coordination groups has been shown to increase ligand affinities[22] and the positive charge on the xanthene ring promotes electron deficiency at the aryl group, consequently decreasing the pK_a values of these chelators.[20]

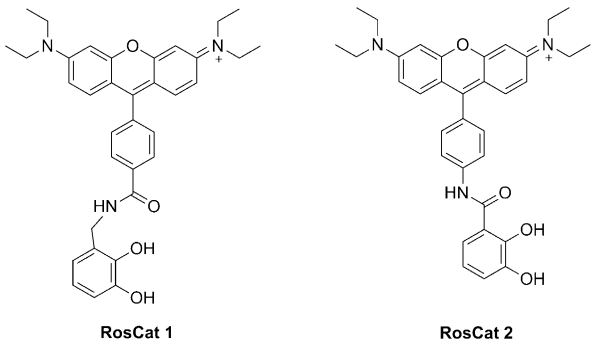

Figure 2. Formulae of catechol-modified rosamine derivatives **RosCat1** and **RosCat2**.

Results and Discussion

Design of ligands

The design of the fluorescent ligands consisted of the covalent linkage of a fluorescent rosamine reporter with a strong chelating receptor based on a catechol ring. The connectivity of both identities was based on the amide linkage, thus providing the synthesis of two ligands: 1) **RosCat1** resulted from the condensation of rosamine–CO_2H with the NH_2CH_2–catechol derivative, thereby presenting the C=O functionality directly linked to the phenyl ring of the rosamine unit; 2) **RosCat2** resulted from the condensation of rosamine–NH_2 with the CO_2H–catechol derivative, thus presenting the C=O functionality directly attached to the catechol unit. Note that **RosCat1** has one additional CH_2 group attached to the catechol, which gives more flexibility to the ligand and increases the distance of the amide linkage to the OH groups of the catechol unit.

Synthesis

The rosamine precursors **1** and **2** (R = CO_2H and NO_2, respectively; Scheme 1) were prepared by using a reported methodology[19] that involves a two-step sequence: 1) the microwave-assisted condensation of 3-(diethylamino)phenol with formylbenzoic acid and 4-nitrobenzaldehyde and 2) oxidation with chloranil. For both rosamines, the condensation step was carried out with water as the solvent, thus facilitating the

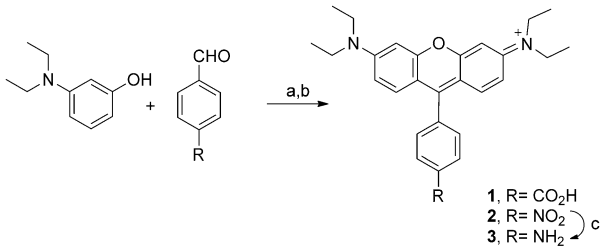

Scheme 1. Microwave-assisted synthesis of rosamines **1**–**3**. Reagents and conditions: a) water, *p*-TsOH, MW; b) chloranil, MW; c) 1. H_2, Pd/C, ethanol or 2. cyclohexene, Pd/C, ethanol, MW. *p*-TsOH = *para*-toluenesulfonic acid, MW = microwave.

isolation of the reaction crude by means of a simple filtration process (see the Supporting Information). The reduction of rosamine **2** to the corresponding amine derivative **3** ($R = NH_2$) was performed by using two protocols: 1) Pd/C catalyzed hydrogenation in a hydrogen atmosphere over 15 hours to furnish the product in 20% yield or 2) the use of cyclohexene as a hydrogen donor in the presence of a catalytic amount of Pd/C in ethanol and under closed-vessel microwave-irradiation conditions (130 °C, 20 min) to give a 66% yield. Note that a significant rate enhancement of the reaction outcome was achieved in the latter protocol.

Although the condensation of fluorescent rosamine **1** with 2,3-dibenzyloxybenzylamine (Scheme 2) with *N*,*N*′-dicyclohexylcarbodiimide (DCC) and *N*-hydroxysuccinimide as coupling agents (RT, 24 h) furnished conjugate **4** in 27% yield, the same reaction with EDC, HOBt, and DIPEA as a base[21] under closed-vessel microwave conditions (75 °C, 20 min) allowed a higher yield of conjugate **4** (77%). Final removal of the benzyl ether protecting groups of **4** was achieved by using BCl_3 in dichloromethane in an argon atmosphere, thus affording the expected ligand **RosCat1**.

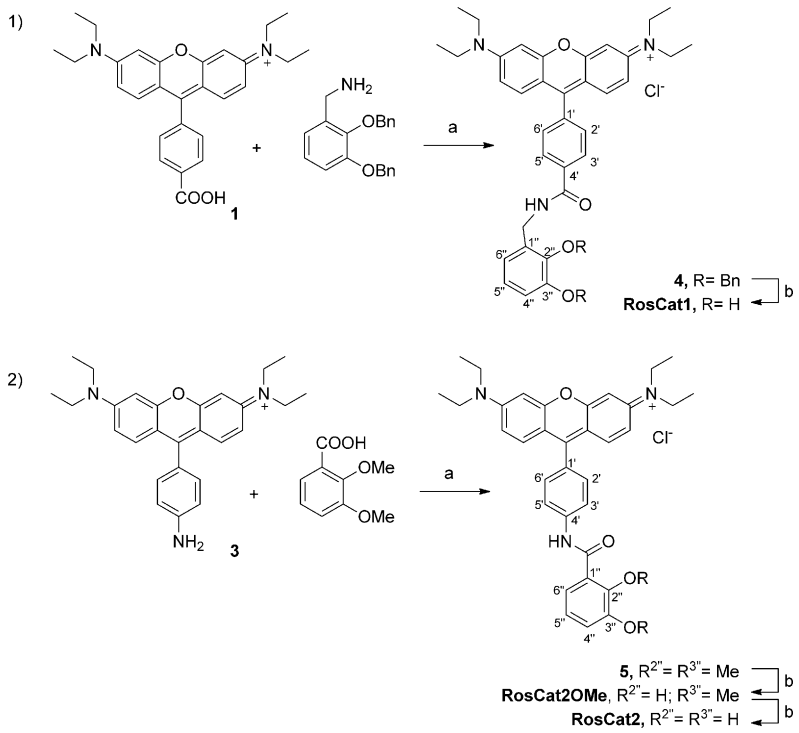

Scheme 2. Synthetic routes for 1) **RosCat1** and 2) **RosCat2OMe** and **RosCat2**. a) EDC, HOBt, DIPEA, anhydrous DMF, MW; b) BCl_3, CH_2Cl_2. DIPEA = *N*,*N*-diisopropylethylamine, EDC = *N*-(3-dimethylaminopropyl)-*N*-ethylcarbodiimide hydrochloride, HOBt = hydroxybenzotriazole.

RosCat2 was prepared by using a similar approach (Scheme 2). The condensation of rosamine **3** with dimethoxybenzoic acid afforded conjugate **5** in 45% yield. The removal of the methyl ether protecting groups was also carried out by using BCl_3 in dichloromethane. It was interesting to verify that **RosCat2OMe** was isolated as the main product of the reaction. According to NMR spectroscopic and mass-spectrometric analysis of **RosCat2OMe**, only the 2′′-methyl ether group was removed, thus leaving the 3′′-methyl ether protecting group intact. A further reaction was carried out with a larger excess of BCl_3 to remove both protecting groups of the ligand, thereby affording the desired **RosCat2**.

Both fluorescent ligands were characterized by ^1H and ^{13}C NMR, UV/Vis, and fluorescence spectroscopic and mass-spectrometric analysis. Moreover, the structure of **RosCat1** was confirmed by means of single-crystal X-ray diffraction studies. The mass spectra of both ligands show the corresponding molecular ion [M^+] as a base peak at *m*/*z* 564.3 and 550.3 for **RosCat1** and **RosCat2**, respectively.

NMR characterization

The NMR spectra were obtained in [D_6]DMSO and [D_4]MeOH (as aprotic and protic solvents, respectively) to extract structural information about the influence of the electronic properties of the amide functionality in **RosCat1** and **RosCat2**. In the ^1H NMR spectrum of **RosCat1** in [D_6]DMSO (Figure 3a), it is noticeable that the C=O function, which is directly attached to the phenyl ring of the rosamine, has a strong deshielding effect on the ^1H chemical shifts on the H-3′ and H-5′ protons, which appear at $\delta = 8.20$ ppm.

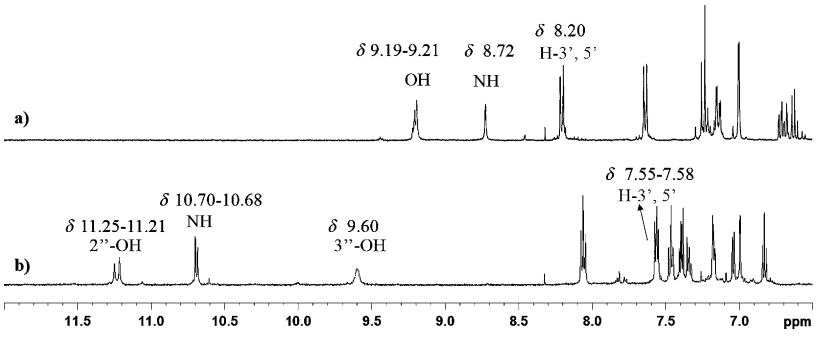

Figure 3. Partial ^1H NMR spectra of a) **RosCat1** and b) **RosCat2** in [D_6]DMSO.

The ^{1}H chemical shifts of the most deshielded protons are 1) a singlet at $\delta = 8.72$ ppm, attributed to the NH resonance and 2) a multiplet at $\delta = 9.19$–9.21 ppm, attributed to the two OH protons. In the aliphatic region of the spectrum, the signal that corresponds to the resonance of the CH_2 group, which appears at $\delta = 4.50$ ppm in [D_6]DMSO and at $\delta = 4.60$ ppm in [D_4]MeOH, showed a HMBC correlation with a carbon atom at $\delta = 168.5$ ppm, which was attributed to the C=O bond of the amide group and also with more three carbon atoms: 1) one at $\delta = 120.5$ ppm, assigned as C-6″; 2) one at $\delta = 125.3$, assigned as C-1″; and 3) one at $\delta = 143.7$ ppm, which corresponds to C-2″.

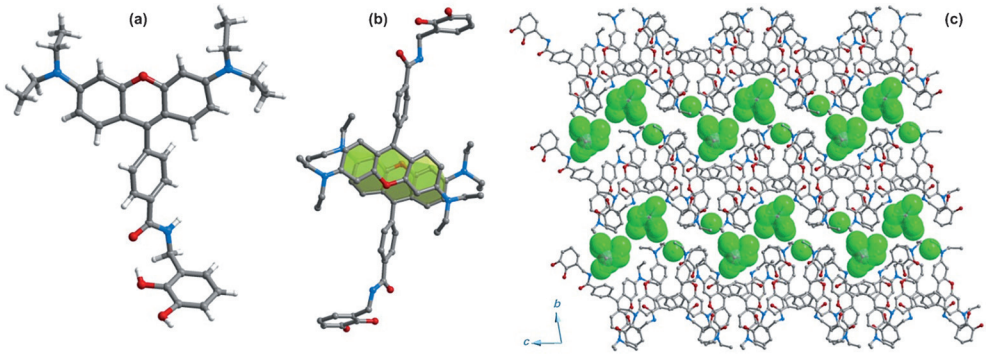

Figure 4. Selected features of the crystal structure of **RosCat1**·Cl·CH_3Cl. a) **RosCat1** ligand; b) π···π stacking involving two adjacent organic molecules; c) extended packing viewed in the [100] direction of the unit cell. The hydrogen atoms have been omitted for clarity. C, gray; H, white; Cl, green; N, blue; O, red.

Relative to **RosCat2**, the ^{1}H NMR spectrum exhibits a signal that corresponds to the H-3′ and H-5′ resonances, which are more shielded at $\delta = 7.55$–7.58 ppm (Figure 3b). The most deshielded protons are 1) a singlet at $\delta = 9.60$ ppm, attributed to the 3″-OH proton; 2) a multiplet at $\delta = 10.70$–10.68 ppm, as the NH resonance, which is in agreement with the chemical shifts observed for other catecholamides;[24] and 3) a multiplet that arises at $\delta = 11.25$–11.21 ppm, assigned as the most acidic 2″-OH proton. This chemical shift for 2″-OH is consistent with a hydrogen-bonding interaction of 2″-OH with the oxygen atom of the amide linkage. In addition, the NH signal showed a HMBC correlation with a carbon atom at $\delta = 168.1$ ppm, which was attributed to the C=O bond of the amide group, and a carbon atom at $\delta = 121.1$ ppm, assigned as C-3′ and C-5′.

X-ray structure studies

Several attempts were carried out to obtain single crystals of both ligands with different crystallization techniques and solvents; however, only **RosCat1** produced very small pink needle crystals, which were obtained by slow evaporation of a solution of **RosCat1** in a mixture of methanol and $CHCl_3$. As consequence of the small dimensions of the crystals and their inherently weak diffraction, it was only possible obtain to the crystal structure by using synchrotron radiation (see the Experimental Section for detailed information).

The crystal structure was determined to have triclinic crystal system and the space group *P*1, thus unequivocally confirming the synthesis of the ligand **RosCat1** (Figure 4a). The asymmetric unit cell (asu) comprises four cationic organic molecules, four chloride anions, and four $CHCl_3$ molecules as the crystallization solvent. The **RosCat1** ligand revealed a structural arrangement in which a xanthene moiety was present and the adjacent phenyl ring was considerably twisted (the dihedral angle between both the average planes defined by these two aromatic groups is 50.266°). Furthermore, the two OH groups of the catechol ring had the same orientation as the C=O group, with an interaction between the adjacent hydroxy and C=O groups through intermolecular O-H···O hydrogen bonds in the four crystallographic independent molecules (Figure 4a).

The structural arrangement of the **RosCat1** ligand is definitely influenced and stabilized by an extensive network of intermolecular interactions, mainly hydrogen bonds and π···π stacking. Neighboring molecules interact directly through π···π contacts that involve the xanthene groups (green shadow in Figure 4b), with the two molecules in antiparallel positions. Furthermore, the **RosCat1** ligands are involved in an extensive intermolecular hydrogen-bonding network with the chloride anions, the $CHCl_3$ molecules of crystallization, and O-H···Cl and N-H···Cl interactions. In fact, the organic molecules act principally as donors, through the hydroxy groups of the catechol rings and the amide groups, with all the intermolecular interactions leading to the formation of a 3D supramolecular network (not shown). The extended packing of the **RosCat1** molecules in the [100] direction of the unit cell shows layers that run along the *c* axis in a zig-zag arrangement, in which the charge-balancing chloride anions and the solvent molecules occupy the space between these organic layers (Figure 4c).

Spectroscopic properties

To investigate the optical spectroscopic properties of both ligands and their solvent dependence, we carried out UV/Vis absorption and fluorescence studies in protic (i.e., ethanol and methanol) and nonprotic (i.e., dichloromethane) solvents. Moreover, considering that both ligands show low solubility in H_2O and knowing that catechol derivatives exhibit interesting properties in DMSO,[22] we decided to investigate different H_2O/DMSO mixtures (i.e., H_2O/DMSO = 30:70 and 90:10; the results are summarized in Table 1 and Figure S23 in the Supporting Information). The maximum wavelengths of the absorption bands in dichloromethane and ethanol/methanol are very similar for both ligands (within $\lambda = 556$–563 nm), but a bathochromic shift of the UV/Vis absorption maximum is observed in the solvent mixture H_2O/DMSO = 30:70 ($\lambda = 566$–569 nm). This bathochromic shift is presumably caused by hydrogen-

Table 1. Experimental and calculated UV/Vis and fluorescence spectroscopic properties of **RosCat1** and **RosCat2**.[a]

Ligand	Solvent	Exptl $\lambda_{abs,max}$ [nm]	ε [$\times 10^4$ M^{-1} cm^{-1}]	Calcd $\lambda_{abs,max}$ [nm]	Exptl $\lambda_{em,max}$ [nm]	φ_F
	CH_2Cl_2	563	4.9	513	583	0.14
	C_2H_5OH	560	4.7		583	0.18
	CH_3OH	561	4.6		584	0.18
RosCat1	H_2O/DMSO 30:70	569	4.3		595	0.04
	H_2O/DMSO 90:10	564	0.61	523[b]	591	–
	CH_2Cl_2	559	4.3	510	575	0.04
	C_2H_5OH	556	4.4		578	0.04
	CH_3OH	559	4.8		577	0.04
RosCat2	H_2O/DMSO 30:70	566	3.3		588	0.01
	H_2O/DMSO 90:10	570	0.54		597	–

[a] The fluorescence quantum yield φ_F was determined.[24] [b] Calculated in H_2O.

bond formation and deprotonation of the catechol units and has been observed for other catechol derivatives.[23]

The simulated absorption spectrum, obtained by using time-dependent DFT (TD-DFT) calculations, of the most stable conformer of **RosCat1** in water showed the lowest energy band at $\lambda = 523$ nm, which involves the HOMO→LUMO transition (Table 1). This value is in agreement with the experimental spectrum obtained in a mixture of H_2O/DMSO = 90:10, with $\lambda_{abs,max} = 564$ nm. The observed difference can be attributed to the fact that the model does not consider the microscopic interactions between the solvent molecules and the solute, including the hydrogen-bond formation,[25] which is highly relevant for our ligands. On the other hand, the calculations also reveal that the absorption values in dichloromethane are very similar for both ligands, but are slightly lower than in water for **RosCat1**, which is consistent with the results obtained experimentally.

A redshift in fluorescence is observed for the maximum wavelengths of the emission bands in the H_2O/DMSO mixtures for both ligands. Our experimental data show that the fluorescence quantum yields also vary with the polarity of the solvents and are strongly influenced by the amide linkage and the nature of the substituent introduced at the 4′ position of the rosamine scaffold. In dichloromethane, ethanol, and methanol, the calculated quantum yields are relatively low ($\phi_F = 0.04$) for **RosCat2**, but higher for **RosCat1** (within the range $\phi_F = 0.14$–0.18).

The minor ϕ_F values achieved for **RosCat2** are in agreement with previous results, in which the introduction of a nitrogen atom at the 4′ position of the rosamine phenyl ring caused a decrease in fluorescence emission.[19] Particularly attractive is the fourfold increase in ϕ_F value determined for **RosCat1**, which could be a relevant feature for potential fluorescent-sensing applications. An increase of the solvent polarity by using a mixture of H_2O/DMSO = 30:70 results in a dramatic decrease in the fluorescence quantum yields (within the range $\phi_F = 0.04$–0.01) for both ligands, which leads to nearly complete suppression of emission for polar solvents, as previously reported for other families of catechol derivatives.[22]

DFT calculations

DFT calculations were performed for **RosCat1** and **RosCat2**, and the optimized structures of two conformers of the ligands are depicted in Figure 5. The analysis of the results predict that, in both cases, the conformer on the left, with an intramolecular hydrogen bond between the carbonyl and the hydroxy hydrogen atom, is more stable than the conformer with a hydrogen bond between the amide hydrogen atom and the hydroxy oxygen atom, which is in agreement with the NMR spectroscopic analysis and X-ray studies of **RosCat1** (Figure 4). This finding suggests that these conformations are the most suitable to chelate the iron ion.

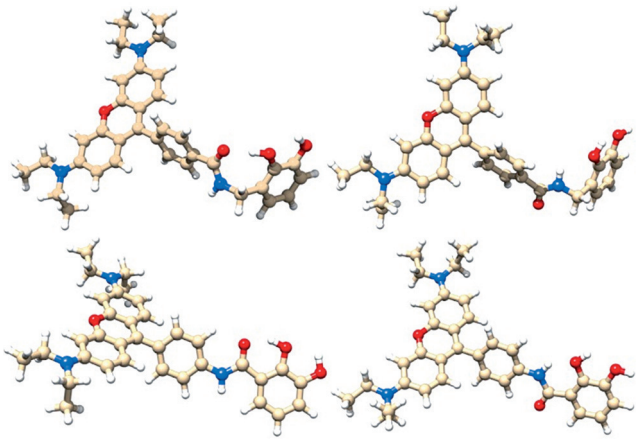

Figure 5. Optimized structures obtained by using DFT calculations of two conformers of **RosCat1** (top) and **RosCat2** (bottom).The conformers on the right are less stable by about 14 kJ mol^{-1}, both in water and dichloromethane.

Fe^{III}-binding properties

All attempts to obtain single crystals of the Fe^{III} complexes of both ligands were unsuccessful in spite of many assays performed that used different crystallization techniques and solvents. Thus, mass-spectrometric studies and theoretical calculations were conducted to elucidate the iron coordination modes for both ligands. The response of the probe with increasing amount of Fe^{III} ions was studied by means of fluorescence spectroscopy.

Considering the most stable conformers obtained for **RosCat1** and **RosCat2**, the coordination geometry at the iron center may involve 1) the amide oxygen atom and the catecholic *ortho*-oxygen atom (i.e., "salicylate-type" coordination) or 2) the two catecholic oxygen atoms ("catecholate-type" coordination; Figure 6).

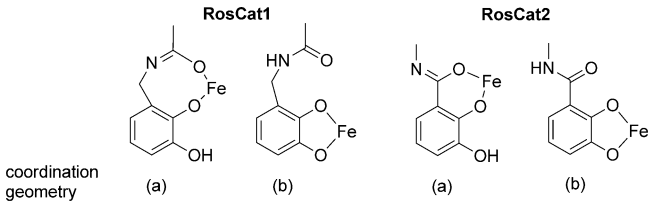

Figure 6. Probable coordination geometries of **RosCat1** and **RosCat2** with Fe^{III} ions.

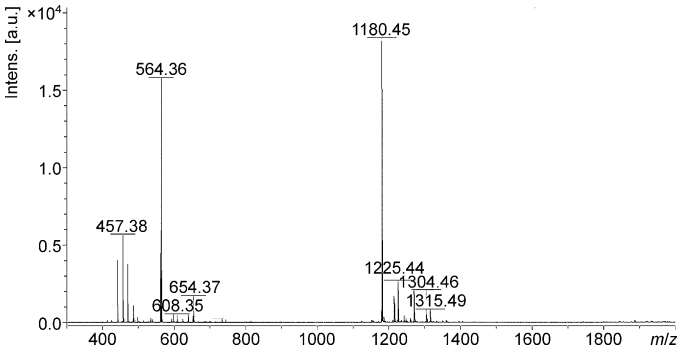

Figure 7. MALDI-TOF mass spectrum of **RosCat1** after the addition of Fe^{III} ions (full spectra).

RosCat1 possesses an unusual inverted amide function that, to the best of our knowledge, has not been explored before in coordination studies with iron and other transition-metal ions. This unconventional amide binding imposes the formation of an eight-membered ring upon chelation, if the amide oxygen atom also participates in iron coordination.

Mass-spectrometric studies

Tandem mass-spectrometric analysis of the iron complexes was performed to obtain empirical evidence of complex formation and the iron coordination mode. Matrix-assisted laser desorption ionization (MALDI) was used and *trans*-2-[3-(4-*tert*-butylphenyl)-2-methyl-2-propenylidene]malononitrile (DCTB) was the chosen matrix. The mass spectra obtained for the ligands are presented in the Supporting Information (see Figures S24 and S25).

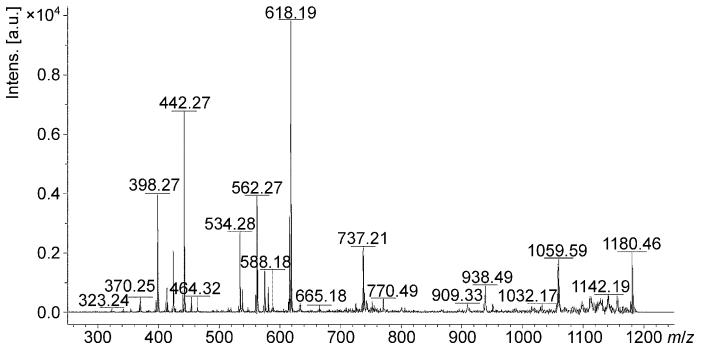

Figure 8. Tandem mass spectra (MALDI-TOF/TOF-MS) of the Fe/**RosCat1** complex $[FeL_2]^+$ (*m/z* 1080.48).

Figure 7 shows the mass spectra obtained for the mixture of iron chloride and **RosCat1** (L). The two predominant ions at *m/z* 564.36 and 1180.45 correspond to the free ligand and the ferric **RosCat1** complex $[FeL_2]^+$, respectively. The FeL_3 complex was observed as peak at *m/z* 1743.78 $[FeL_3H]^+$ with a very low intensity (see Figure S26 in the Supporting Information). It is dubious whether the spectrum depicted in Figure 7 reports the solution speciation or reflects the very different ionization/desorption efficiencies of the species present in the MALDI target-plate spot. We adopted an aprotic matrix (i.e., DCTB) under nonacidic conditions because the acidification of the mixture would prevent formation of the iron complex and its observation. The FeL_3 complex is expected to be the most abundant species in solution under such experimental conditions, but it occurs as a neutral species, thus requiring the transfer of a proton for ionization, whereas $[FeL_2]^+$ naturally occurs as an ion. Furthermore, it is conceivable that the most favorable ionization mechanism for FeL_3 is not simple protonation, but the loss of a ligand to generate the $[FeL_2]^+$ ion, thus explaining the similar intensities observed for the free ligand and the $[FeL_2]^+$ complex (Figure 7).

MALDI-TOF/TOF-MS (MS^2) of the ion with the peak at *m/z* 1743.78 ($[Fe^{III}L_3H]^+$) and the structure of the main fragment ions are presented in the Supporting Information (see Figure S27 and Scheme S2). The main spectral features reveal the dissociation of the **RosCat1** ligand, which originated $[Fe(I)L_2H_2]^+$ (*m/z* 1182.10) and a catechol-centered radical cation of the free ligand (*m/z* 563.39). Additional fragmentation pathways include bond cleavage near the bound amide group to generate rosamine-containing fragments (e.g., *m/z* 443.25) and its counterpart, namely, an iron complex with a benzoquinone-type structure (*m/z* 1301.36). The salicylate nature of the ferric ion coordination was only confirmed with the fragmentation of the $[FeL_2]^+$ ion (*m/z* 1180.45; Figure 8). A characteristic feature of the fragmentation pattern of this ion was the cumulative loss of methyl and methylene groups (−15 and −14, respectively), which can be clearly detected in the spectrum as a group of low intensity peaks close to the parent ion. In the spectrum, the detection of a $[Fe^{II}L]^+$ complex (*m/z* 618.19) and several rosamine- and rosamine amide-containing fragments (peaks at below *m/z* 600) is also evident. However, only the ions at *m/z* 1059.59 and 938.46 provide clear evidence for iron coordination through the amide oxygen atom (Scheme 3). The peak at *m/z* 1059.59 corresponds to a mixed Fe^{II} complex with a **RosCat1** ligand and a remaining rosamine amide molecule. The homolytic fragmentation of the N–CH_2 (catechol) bond led to the release of the catechol moiety and the reduction of the metal center. The ion at *m/z* 938.46 results from the loss of a second catechol unit, thus leaving a Fe^{I} center bound to two rosamine amide molecules. Whenever fragmentation resulted in the release of rosamine, the resulting iron complex retained the "amide" moiety, with the oxygen atom anchored to the iron center (Scheme 3; *m/z* 737.17). We believe that the previ-

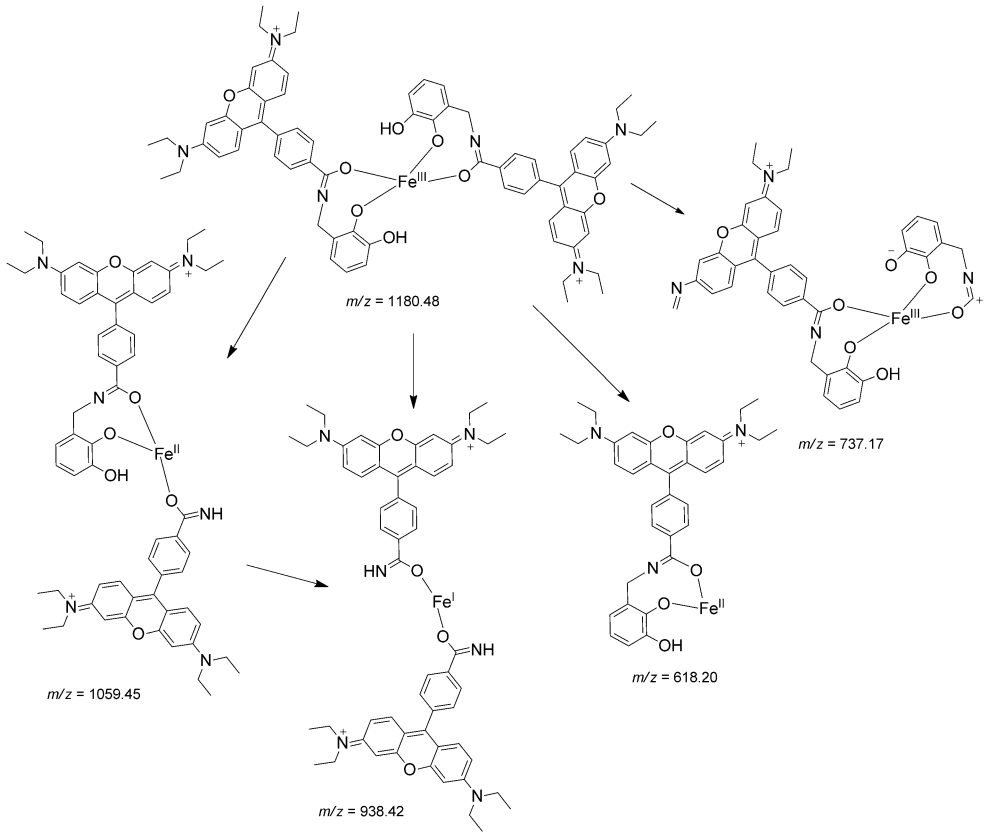

Scheme 3. Chemical structure of the collision-induced fragments of the Fe/**RosCat1** complex $[FeL_2]^+$ (*m/z* 1180.48).

ously described ions are diagnostic for a "salicylate-type" coordination.

Analogous evidence was gathered for the ferric complexes with **RosCat2** (see Figure S28 in Supporting Information for the full MS spectrum obtained for the Fe/**RosCat2** mixture) and is similar to that observed for **RosCat1** with the free ligand and $[FeL_2]^+$ complex (*m/z* 550.26 and 1152.48, respectively) as the main spectral features. The $[FeL_3H]^+$ complex can be observed as a low-intensity peak at *m/z* 1701.73. The collision-induced dissociation of the ion at *m/z* 1701.73, and the chemical structures of the fragment ions are presented in the Supporting Information (see Figure S29 and Scheme S3). Diagnostic evidence for the participation of the amide oxygen atom in metal coordination is provided by the ion at *m/z* 865.54, which corresponds to a Fe^{I} center coordinated by two rosamine residues through the amide oxygen atom.

Dissociation of the $[FeL_2]^+$ ion (*m/z* 1152.48) resulted in the formation of a $[Fe^{II}L]^+$ complex (*m/z* 604.28) and several Fe^{III} complexes containing a salicylate-type structure (i.e., catechol amide radical anion) and a **RosCat2** unit with losses of methylene and ethylene groups (*m/z* 739.33, 710.28, and 683.32; Figure 9 and Scheme 4.

Altogether, the preponderance of the iron complexes with the remaining salicylate-type catechol amide moiety suggests that a preferred coordination geometry involves the amide oxygen atom, but definitive confirmation is provided by the ion at *m/z* 1017.66, which corresponds to the loss of a catechol unit and the formation of a characteristic Fe^{II}/**RosCat2** complex bound to rosamine residues through the amide oxygen atom. Formation of these characteristic structures with rosamine residues bound to the metal ion center through the amide oxygen atom reflects an initial engagement of this moiety in iron coordination, which would facilitate the loss of the catechol unit.

The mass spectrum of the monoprotected ligand **RosCat2OMe** after the addition of Fe^{III} ions revealed at a peak at *m/z* 1180.48 that corresponds to the ferric complex $[FeL_2]^+$, with the loss of two protons relative to the expected complex (see Figure S30 in the Supporting Information). Because this ligand carries the 3′′-methyl ether protecting group, deprotonation can only occur at the amide function, which is therefore the -CO═N-

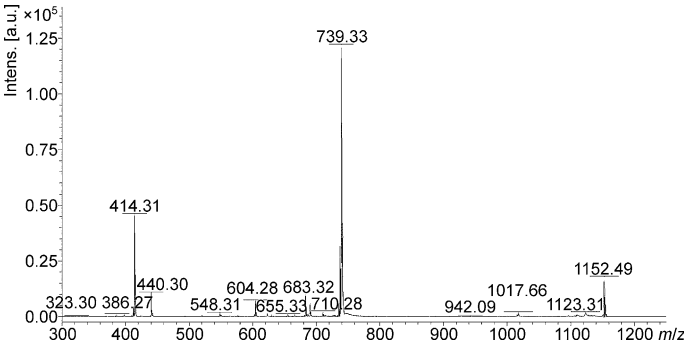

Figure 9. Tandem mass spectra (MALDI-TOF/TOF-MS) of the Fe/**RosCat2** complex $[FeL_2]^+$ (*m/z* 1052.48).

species. By analogy, it is also anticipated that similar deprotonation reactions occur in both **RosCat1** and **RosCat2** ligands.

Theoretical calculations

Semiempirical calculations, carried out by using the PM6 method, were performed to investigate the structures of the octahedral complexes that can be obtained through bidentate coordination of three **RosCat1** or **RosCat2** ligands to the Fe^{III} ion. Neutral complexes are obtained after double deprotona-

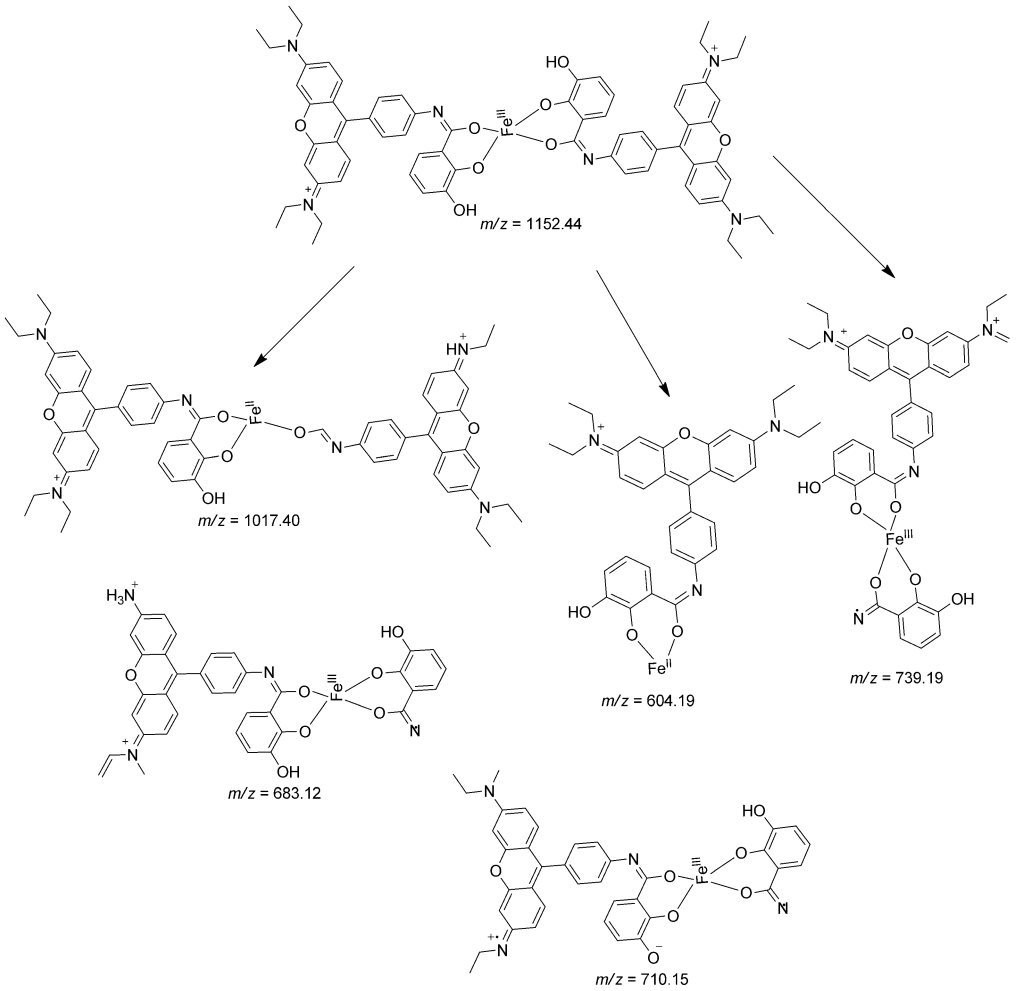

Scheme 4. Chemical structure of the collision-induced fragments of the Fe/**RosCat2** complex $[FeL_2]^+$ (*m/z* 1052.48).

tion of the amide group and one of the catechol hydroxy groups or both of the catechol hydroxy groups.

The results obtained predict that for **RosCat1** the isomer with the iron center coordinated by the two catechol oxygen atoms (top-right structure in Figure 10) is less stable than the isomer with the iron center coordinated by the amide oxygen and the catechol *ortho*-oxygen atoms (top-left structure in Figure 10) by about 129 kJ mol^{-1}. Therefore, only the isomer on the left of Figure 10 should be present in solution for **RosCat1**, thus excluding the coordination by the two catechol oxygen atoms. Also, the most stable structure in the case of **RosCat2** occurs with chelation through the amide oxygen and catechol *ortho*-oxygen atoms, which is more stable by about 30 kJ mol^{-1} than the structure with the chelation through the two catechol oxygen atoms (bottom structures in Figure 10).

The results obtained through the structural support of the semiempirical calculations described above strongly support the results obtained by mass-spectrometric analysis. Notwithstanding the inability to obtain crystal structures for the Fe^{III} complexes, we believe that the cross validation provided by the theoretical and experimental methods strongly suggests that both ligands coordinate this metal ion through a salicy-

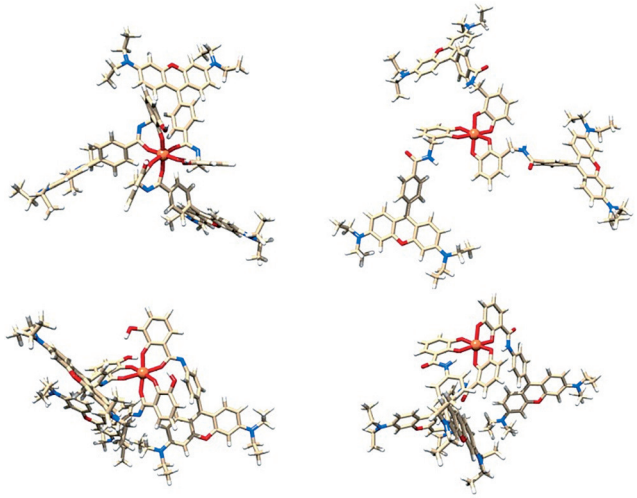

Figure 10. Optimized structures obtained by using semiempirical PM6 calculations of two isomers of the Fe^{III} octahedral complexes with **RosCat1** (top) and **RosCat2** (bottom). The isomers on the right with the "catecholate-type" coordination are less stable by about 129 (top) and 30 kJ mol^{-1} (bottom) for the **RosCat1** and the **RosCat2** ligands, respectively.

late-type geometry. The salicylate-type coordination prevails despite the inverted amide function present in **RosCat1**, and the resulting unusual eight-membered ring structure. Contrary to that described for enterobactin,[14–16] the mass-spectrometric results indicate that amide deprotonation occurs upon iron coordination by both ligands. This effect most probably results from a reduction in the pK_a value of the amide group induced by the electron-withdrawing effect of the rosamine moiety and is expected to favor the ability of the amide oxygen atom to participate in metal-ion coordination.[20]

Fluorescence-intensity quenching study

Considering the higher quantum yield values obtained for **RosCat1**, our previous studies,[9,26] and the potential importance of these ligands in monitoring Fe^{III} species in biological fluids, we performed a fluorescence quenching study of **RosCat1** in the presence of Fe^{III} ions in MOPS (pH 7.4; Figure 11).

The interaction of **RosCat1** with Fe^{III} ions was investigated by examining the variation observed in the fluorescence intensity of the ligand by increasing concentrations of the metal ion with a fixed concentration of the ligand. Evidence of the corresponding metal-complex formation in solution can be provided by observation of significant quenching of fluorescence intensity. Figure 11 presents the change in the emission-fluorescence intensity of **RosCat1** with increasing concentrations of Fe^{III} ions. From analysis of Figure 11, we can conclude that the quenching effect of Fe^{III} ions on **RosCat1** is almost complete at a metal/ligand ratio of 1:3, as expected from similar studies,[8,9] and the percentage of fluorescence quenching was approximately 93%. The same study was performed in the presence of Cu^{II} ions for **RosCat1**, and a value of fluorescence quenching of approximately 90% was obtained.

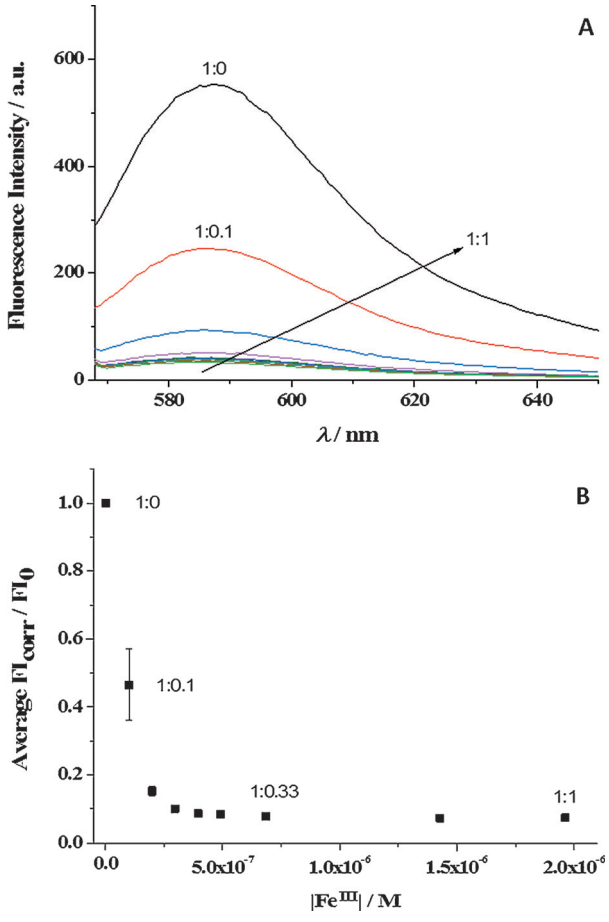

Figure 11. A) Graphical representation the emission-fluorescence intensities of **RosCat1** with increasing Fe^{III} concentrations (2 μM, 4-morpholinepropanesulfonic acid (MOPS), pH 7.4, 25 °C, λ_{exc} = 561 nm). **RosCat1**/metal ratios of 10:1→1:1 were tested. B) Maximum emission-fluorescence intensity (measured at λ_{em} = 586 nm) plotted against the corresponding Fe^{III} concentrations. Measurements were carried out in triplicate.

Considering the levels of low-molecular-weight Cu^{II} and Fe^{III} complexes[27] and the reported complex stability constants of Fe^{III} and Cu^{II} with catechols,[7,28] it is expected that the observation of an emission-fluorescence quenching effect of **RosCat1** in living cells (i.e., under physiological conditions) is associated with the presence of chelatable iron species and not the presence of copper species.

When compared to previously described rhodamine and fluorescein analogues of the catechol-containing receptors **Cat1** and **RhodCat**,[8,9] **RosCat1** presents the highest fluorescence intensity quenching for Fe^{III} ions (i.e., 93 vs. 78 and 75%, respectively).

Other reports on fluorescent probes that show a high affinity for Fe^{III} ions have considered the use of hydroxamates[29] and 3-hydroxy-4-pyridinones (HPO),[30] among other ligands.[31] **RosCat1** compares well with a HPO analogue by presenting much more effective fluorescence-intensity quenching relative to a hydroxypiridinone/rhodamine conjugate synthesized by us (93 vs. 63%).[9]

Hider and co-workers reported a series of fluorescent systems labeled with coumarin/fluorescein as fluorophores in combination with either hydroxypyridinone/hydroxypyranone receptors, in which amide linkages were used in most of the cases.[30] However, 3-hydroxy-4-pyridinone ligands consistently present a slightly lower affinity or fluorescence-intensity quenching for Fe^{III} ions relative to similar catechol derivatives[8] as a result of iron coordination through the two vicinal oxygen atoms of the pyridinone ring.

Considering the results reviewed by Callan and co-workers, **RosCat1** also presents quantum yields and fluorescence intensity quenching that are generically superior to the series of hydroxypyridinones studied.[3]

Conclusion

Fluorescent ligands **RosCat1** and **RosCat2** have been synthesized, and their Fe^{III} coordination chemistry has been explored further. The structural characterization of both ligands performed by NMR spectroscopic analysis and X-ray studies for **RosCat1**, combined with theoretical studies, revealed that the amide oxygen atom had the same orientation as the two catechol oxygen atoms. In both ligands, the adjacent hydroxy and C=O groups interact through intermolecular hydrogen bonds, thus suggesting that this conformation is the most suitable to

chelate iron ions. The coordination geometry of the iron center provided by both ligands was elucidated by mass-spectrometric analysis and semiempirical calculations, which revealed that a "salicylate-type" coordination to the Fe^{III} center takes place.

The optical properties reported herein show that the **RosCat1** ligand exhibited more interesting fluorescent properties than **RosCat2**. Therefore, the fluorescence response of **RosCat1** to the presence of Fe^{III} ions in aqueous buffer at physiological pH values showed concentration-dependent quenching of the fluorescence intensity.

Our results have shown that the use of an inverted amide function with an additional methylene unit is a suitable synthetic solution for the conjugation of fluorescent moieties with the catechol receptor, thus preserving fluorescent properties that are absent when the most common amide configuration is used. We believe that **RosCat1** presents itself as a promising prototype molecule for the design of Fe^{III} probes that take advantage of the high affinity and selectivity provided by its catechol unit.

Experimental Section

Reagents and solvents were purchased as reagent grade and used without further purification, unless otherwise stated. NMR spectra were recorded on a Bruker Avance III 400 spectrometer operated at 400.15 and 100.62 MHz for the ^1H and ^{13}C nuclei and equipped with pulse-gradient units capable of producing magnetic-field pulsed gradients in the *z* direction of 50.0 G cm^{-1}. For ligand **RosCat2**, the NMR spectra were recorded on a Bruker Avance III HD 600 spectrometer operated at 600.13 and 150.92 MHz for the ^1H and ^{13}C nuclei and equipped with pulse-gradient units capable of producing magnetic-field pulsed gradients in the *z* direction of 6.57 G cm^{-1}. Two-dimensional $^1H/^1H$ correlation spectra (COSY), gradient-selected $^1H/^{13}C$ heteronuclear single quantum coherence (HSQC), and $^1H/^{13}C$ heteronuclear multiple-bond coherence (HMBC) spectra were acquired by using standard Bruker software. Mass spectra were acquired by Unidade De Espectrometria De Masas (Santiago de Compostela, Spain) and microanalyses were acquired by Unidad De Análisis Elemental (Santiago de Compostela, Spain). Flash chromatography was carried out on silica gel Merck (230–400 mesh). Electronic absorption spectra were recorded on a Varian Cary bio50 spectrophotometer thermostabilized at 25.0 °C, and fluorescence measurements were performed on a Varian Cary Elipse spectrofluorometer equipped with a constant-temperature multicell cell holder (25.0 ± 0.1 °C), with 5 mm slits width for excitation and emission. Mass spectra were acquired on a Bruker UltrafleXtreme MALDI-TOF/TOF equipped with a smartbeam laser (200 Hz; Bruker Daltonik GmbH, Bremen, Germany).

Synthesis

Synthesis of conjugate 4: A mixture of rosamine 1 (0.05 mmol, 20.7 mg), 2,3-dibenzyloxybenzylamine[8] (0.09 mmol, 28.7 mg), EDC (0.05 mmol, 8.1 mg), HOBt (0.05 mmol, 7.1 mg), and DIPEA (0.11 mmol, 0.02 mL) in dry DMF (0.3 mL) was placed in a reaction vial (10 mL), which was closed in a nitrogen atmosphere and placed in the cavity of a CEM microwave reactor. The reaction vial was irradiated (1 min up to 75 °C and 20 min at 75 °C at a power maximum of 100 W). The resulting mixture was purified by flash chromatography with $CHCl_3$ and then $CHCl_3$/methanol (9:1) as the eluents. Conjugate **4** was obtained in 77% yield (27.9 mg). ^1H NMR ($CDCl_3$, 400.15 MHz): $\delta = 1.33$ (t, 12H, $J = 7.2$ Hz; 4×CH_2CH_3); 3.63 (q, 8H, $J = 7.2$ Hz; 4×CH_2CH_3), 4.73 (d, 2H, $J = 6.0$ Hz; $NHCH_2$), 5.13 (s, 2H; 3″-$CH_2C_6H_5$), 5.18 (s, 2H; 2″-$CH_2C_6H_5$), 6.81 (d, 2H, $J = 2.3$ Hz; H-4, H-5), 6.89 (dd, 2H, $J = 9.6$ and $J = 2.3$ Hz; H-2, H-7), 6.92 (dd, 1H, $J = 8.0$ and $J = 1.2$ Hz; H-4″), 7.01 (dd, 1H, $J = 8.0$ and $J = 7.6$ Hz; H-5″), 7.15 (d, 1H, $J = 7.6$ Hz; H-6″), 7.30–7.40 and 7.46–7.48 (2 m, 14H; H-Ar), 8.20 (d, 2H, $J = 8.0$ Hz; H-3′, H-5′), 8.40 ppm (t, 1H, $J = 6.0$ Hz; $NHCH_2$); ^{13}C NMR ($CDCl_3$, 100.62 MHz): $\delta = 12.8$ (CH_2CH_3), 39.5 ($NHCH_2$), 46.3 (CH_2CH_3), 71.2 and 75.0 ($CH_2C_6H_5$), 96.6 (C-4, C-5), 113.3 (C-4″), 114.4 (C-2, C-7), 122.0 (C-6″), 124.5 (C-5″), 127.7, 128.1 (C-3′, C-5′), 128.5, 128.6, 128.7, 128.8, 129.6, 132.3, 138.0, 142.5 (C-2″), 151.9 (C-3″), 155.7, 158.1, 166.0 ppm (CONH); MS (ESI): *m/z*: 744 [M^+].

Synthesis of conjugate 5: A mixture of rosamine 3 (0.12 mmol, 0.05 g), dimethoxybenzoic acid (0.24 mmol, 0.04 g), EDC (0.25 mmol, 0.04 g), HOBt (0.25 mmol, 0.04 g), and DIPEA (0.24 mmol, 0.04 mL) in dry DMF (0.8 mL) was placed in a reaction vial (10 mL), which was closed in a N_2 atmosphere and placed in the cavity of a CEM microwave reactor. The reaction vial was irradiated (1 min up to 75 °C and 20 min at 75 °C at a power maximum of 100 W). The resulting mixture was purified by flash chromatography with $CHCl_3$/methanol (9:1) as the eluent to afford conjugate **5** in 45% yield (31.6 mg). ^1H NMR ($CDCl_3$, 400.15 MHz): $\delta = 1.36$ (t, 12H, $J = 7.2$ Hz; 4×CH_2CH_3); 3.69 (q, 8H, $J = 7.2$ Hz; 4×CH_2CH_3), 3.97 (s, 3H; OCH_3), 4.10 (s, 3H; OCH_3), 6.86 (d, 2H, $J = 2.4$ Hz; H-4, H-5), 6.98 (dd, 2H, $J = 9.6$ and $J = 2.4$ Hz; H-2, H-7), 7.16 (dd, 1H, $J = 8.4$ and $J = 1.6$ Hz; H-4″), 7.26 (dd, 1H, $J = 8.4$ and $J = 7.8$ Hz; H-5″), 7.43 (d, 1H, $J = 8.4$ Hz; H-3′, H-5′), 7.49 (d, 2H, $J = 9.6$ Hz; H-1, H-8), 7.82 (dd, 1H, $J = 7.8$ and $J = 1.6$ Hz; H-6″), 8.17 (d, 2H, $J = 8.4$ Hz; H-2′, H-6′), 10.45 ppm (s, 1H; NH); ^{13}C NMR ($CDCl_3$, 100.62 MHz): $\delta = 13.6$ (CH_2CH_3), 47.1 (CH_2CH_3), 57.1 and 62.8 (2× OCH_3), 97.5 (C-4, C-5), 114.2 (C-1a, C-8a), 115.1 (C-2, C-7), 117.1 (C-4″), 121.3 (C-3′, C-5′), 123.8 (C-6″), 125.8 (C-5″), 127.3 (C-1′), 127.9, 131.6 (C-2′, C-6′), 133.1 (C-1,8), 141.6 (C-4′), 148.3 (C-2″), 153.6 (C-3″), 156.4 (C-3,6), 158.1 (C-9), 158.9 (C-4a, C-5a), 164.6 ppm (CONH).

Synthesis of RosCat1: A solution of boron trichloride in dichloromethane (1 M, 2 mL) was dropped slowly into an ice-bath-cooled suspension of **4** (0.10 g, 0.14 mmol) in dry dichloromethane (8 mL) in a N_2 atmosphere. The mixture was stirred at room temperature for 18 h. Methanol (18 mL) was added to stop the reaction. After removal of the solvent under vacuum, the residue was precipitated with methanol/acetone to afford **RosCat1** as a deep-violet solid (56.7 mg, 68%). ^1H NMR ([D_6]DMSO, 400.15 MHz): $\delta = 1.22$ (t, 12H, $J = 7.0$ Hz; 4×CH_2CH_3); 3.67 (q, 8H, $J = 7.0$ Hz; 4×CH_2CH_3), 4.50 (d, 2H, $J = 6.0$ Hz; $NHCH_2$), 6.62 (t, 1H, $J = 7.6$ Hz; H-5″), 6.68 (d, 1H, $J = 7.6$ Hz; H-4″), 6.72 (dd, 1H, $J = 7.6$ and $J = 2.0$ Hz; H-6″), 7.00 (d, 2H, $J = 2.3$ Hz; H-4, H-5), 7.14 (dd, 2H, $J = 9.6$ and $J = 2.3$ Hz; H-2, H-7), 7.24 (d, 2H, $J = 9.6$ Hz; H-1, H-8), 7.64 (d, 2H, $J = 8.4$ Hz; H-2′, H-6′), 8.20 (d, 2H, $J = 8.4$ Hz; H-3′, H-5′), 8.72 (br s, 1H; NH), 9.19–9.21 ppm (m, 2H; OH); ^{13}C NMR ([D_6]DMSO, 100.62 MHz): $\delta = 12.5$ (CH_2CH_3), $NHCH_2$ under the DMSO signal, 45.4 (CH_2CH_3), 96.1, 112.6, 114.3, 114.6, 118.7, 125.9, 127.7, 129.6, 131.5, 134.6, 135.5, 142.9, 145.2, 155.2, 155.7, 157.4, 165.8 ppm (CONH); ^1H NMR (CD_3OD, 400.15 MHz): $\delta = 1.31$ (t, 12H, $J = 7.0$ Hz; 4×CH_2CH_3); 3.69 (q, 8H, $J = 7.0$ Hz; 4×CH_2CH_3), 4.60 (s, 2H; $NHCH_2$), 6.67 (dd, 1H, $J = 8.0$ and $J = 7.6$ Hz; H-5″), 6.75 (dd, 1H, $J = 8.0$ and $J = 1.6$ Hz; H-4″), 6.78 (dd, 1H, $J = 7.6$ and $J = 1.6$ Hz; H-6″), 6.98 (d, 2H, $J = 2.4$ Hz; H-4, H-5), 7.07 (dd, 2H, $J = 9.4$ and $J = 2.4$ Hz; H-2, H-7), 7.32 (d, 2H, $J = 9.4$ Hz; H-1, H-8), 7.57 (d, 2H, $J = 8.0$ Hz; H-2′, H-6′), 8.13 ppm (d, 2H, $J = 8.0$ Hz; H-3′, H-5′); ^{13}C NMR (CD_3OD, 100.62 MHz): $\delta = 11.8$ (CH_2CH_3), 39.6 ($NHCH_2$), 45.9 (CH_2CH_3), 96.5 (C-4, C-5), 113.3 (C-1a, C-8a), 114.6 (C-2, C-7), 114.7 (C-4″), 119.7 (C-5″), 120.5 (C-6″), 125.3 (C-1″), 128.0 (C-3′, C-5′), 130.0 (C-2′, C-6′), 131.8 (C-1, C-8), 135.8 (C-

1′), 135.9 (C-4′), 143.7 (C-2″), 145.8 (C-3″), 156.2 (C-3, 6), 156.6 (C-9), 158.5 (C-4a, C-5a), 168.5 ppm (CONH); MS (MALDI-TOF): calcd for $C_{35}H_{38}N_3O_4^+$: *m/z*: 564.29 [M^+]; found: 564.27; elemental analysis (%) calcd for $C_{35}H_{38}ClN_3O_4{\cdot}CHCl_3$: C 60.09, H 5.46, N 5.84; found: C 60.22, H 5.63, N 5.88.

Synthesis of RosCat2OMe: A solution of boron trichloride in dichloromethane (1 M, 2 mL) was dropped slowly into an ice-bath-cooled suspension of **5** (68.9 mg, 0.12 mmol) in dry dichloromethane (10 mL) in a N_2 atmosphere. The reaction mixture was stirred at room temperature for 18 h. Methanol (15 mL) was added to stop the reaction. After removal of the solvent under vacuum, the residue was precipitated with methanol/acetone. ^{1}H NMR (CD_3OD, 400.15 MHz): $\delta = 1.24$ (t, 12H, $J = 6.8$ Hz; $4\times CH_2CH_3$); 3.59 (q, 8H, $J = 6.8$ Hz; $4\times CH_2CH_3$), 3.80 (s, 3H; OCH_3), 6.48 (dd, 1H, $J = 8.0$ and $J = 7.2$ Hz; H-catechol), 6.856–6.861 (m, 3H, H-4, H-5, and H-catechol), 7.00 (d, 2H, $J = 9.2$ Hz; H-2, H-7), 7.29 (d, 2H, $J = 7.0$ Hz; H-3′, H-5′), 7.42 (d, 2H, $J = 9.2$ Hz; H-1, H-8), 7.47 (d, 1H, $J = 8.0$ Hz; H-catechol), 7.90 ppm (d, 2H, $J = 7.0$ Hz; H-2′, H-6′); MS (MALDI): *m/z*: 564.3 [M^+].

Synthesis of RosCat2: Further boron trichloride in dichloromethane (1 M, 2 mL) was added to the resulting residue in dry dichloromethane (5 mL) and under N_2 to remove both protecting groups. The remaining procedure was repeated as previously described. Purification of the crude product was conducted on a Varian ProStar HPLC instrument equipped with a C18 reversed-phase column (Supelco, Ascentis C18, $l = 15$ cm × I.D. = 4.6 mm, 5 μm; Sigma–Aldrich). The crude reaction product was manually injected and separated with a linear gradient from 60% buffer A (0.1% formic acid in water) and 40% buffer B (0.1% formic acid in acetonitrile) to 45% buffer A and 55% buffer B over 20 min at a flow rate of 1 mL min^{-1}. Fractions containing the pure product were obtained from several HPLC runs, collected, and concentrated in a rotatory evaporator. ^{1}H NMR ([D_6]DMSO, 400.15 MHz): $\delta = 1.22$–1.28 (m, 12H; $4\times CH_2CH_3$), 3.66–3.71 (m, 8H; $4\times CH_2CH_3$), 6.83 (t, 1H, $J = 5.3$ Hz; H-5″), 6.99 (d, 2H, $J = 1.6$ Hz; H-4, H-5), 7.04 (d, 1H, $J = 5.3$ Hz; H-4″), 7.17–7.19 (m, 2H; H-2, H-7), 7.38–7.41 (m, 2H; H-1, H-8), 7.45–7.48 (m, 1H; H-6″), 7.55–7.58 (m, 2H, H-3′, H-5′), 8.05–8.08 (m, 2H; H-2′, H-6′), 9.60 (s, 1H; 3″-OH), 10.70–10.68 (m, 1H; NH), 11.25–11.21 ppm (m, 1H; 2‴-OH); ^{13}C NMR ([D_6]DMSO, 100.62 MHz): $\delta = 13.8$ (CH_2CH_3), 45.8 (CH_2CH_3), 96.5 (C-4, C-5), 113.1, 115.0 (C-2, C-7), 115.1, 115.2, 117.1, 118.6 (C-5″), 119.2 (C-4″), 119.5, 121.1 (C-3′, C-5′), 127.1, 127.5, 130.9 (C-2′, C-6′), 131.1, 132.2 (C-1, C-8), 132.8, 140.9, 146.7, 148.0, 148.1, 154.7, 155.5, 156.8, 157.9, 158.5, 168.1 ppm (CONH); ^{1}H NMR (CD_3OD, 400.15 MHz): $\delta = 1.23$ (t, 12H, $J = 7.0$ Hz; $4\times CH_2CH_3$), 3.61 (q, 8H, $J = 7.0$ Hz; $4\times CH_2CH_3$), 6.75 (t, 1H, $J = 8.0$ Hz; H-5″), 6.89 (d, 2H, $J = 2.4$ Hz; H-4, H-5), 6.94 (dd, 1H, $J = 8.0$ and $J = 1.3$ Hz; H-4″), 7.02 (dd, 2H, $J = 9.6$ and $J = 2.4$ Hz; H-2, H-7), 7.40–7.47 (m, 5H; H-1, H-8, H-3′, H-5′, and H-6′), 7.95 ppm (d, 2H, $J = 8.4$ Hz; H-2′, H-6′); MS (MALDI-TOF): calcd for $C_{34}H_{36}N_3O_4^+$: *m/z*: 55:0.27 [M^+]; found 550.29.

Spectroscopic properties

UV/Vis absorption spectra were recorded in quartz cells with a path length of 1 cm at 25.0 ± 0.1 °C. Ligand stock solutions were prepared in DMSO and diluted with CH_2Cl_2, EtOH, MeOH, and mixtures of H_2O/DMSO (30:70 and 90:10) in concentration ranges of 10^{-5}–10^{-7} M for the determination of the molar-absorptivity coefficient (ε). Fluorescence-emission measurements were performed in cuvettes (path length = 1 cm) and all the spectra were recorded at 25.0 ± 0.1 °C, with excitation and emission slit widths of 5 nm, and by using the appropriate excitation wavelengths (λ_{exc}) and ranges for CH_2Cl_2, EtOH, MeOH, and H_2O/DMSO (30:70 and 90:10). The samples absorbance values were kept below 0.1 to minimize reabsorption effects.[32] Quantum-yield determination was performed as described previously.[24,33] Rhodamine B was used as a standard for quantum-yield determination[34] due to its similarity to rosamine compounds. All stock solutions of the compounds were prepared in DMSO, with the final concentration of DMSO below 1% in dichloromethane and ethanol as the final solvents. The absorbance of the solutions was adjusted to approximately 0.5 units and the solutions were diluted by a factor of at least 10. The final absorbance of the solutions was in the range 0.05–0.03.

Fluorescence-intensity quenching

Fluorescence intensity measurements were performed in MOPS buffer (pH 7.4) at 25.0 ± 0.1 °C in cuvettes with a path length of 1 cm with excitation and emission slit widths of 5 nm and the appropriate excitation wavelength (λ_{exc}) and range. Stock solutions of Fe^{III} and Cu^{II} ions were prepared from $Fe(NO_3)_3$ and $Cu(NO_3)_2$, respectively (Sigma-Aldrich) and were stabilized with nitrilotriacetic acid trisodium salt (NTA) at a salt/NTA ratio of 1:5. **RosCat1** and **RosCat2** solutions were prepared by dilution of a known volume of the DMSO stock solution in MOPS buffer to achieve final concentrations of 2 and 3 μM, respectively. The DMSO percentage in the final aqueous solutions was less than 1% of the total volume. The ligand solutions were mixed with increasing amounts of the metal stock solution in molar ratios of 10:1→1:3 of **RosCat1** and **RosCat2** ligand/metal ion. The fluorescence intensities were always corrected for dilution.

Synchrotron microcrystal X-ray diffraction studies

The microcrystalline material of **RosCat1**·Cl·$CHCl_3$ was harvested from a crystallization vial and immersed in highly viscous paratone oil. Several microcrystalline particles were mounted on Hampton Research CryoLoo,[35] and inspected under the synchrotron radiation beam at the Swiss–Norwegian BM01a beamline (European Synchrotron Radiation Facilities (ESRF), Grenoble, France) until the collected images resembled diffraction patterns typical of a single crystal. The complete data were collected at 100(2) K on the multipurpose Pilatus@SNBL diffractometer equipped with a Pilatus 2M detector by using highly monochromatic synchrotron radiation at $\lambda = 0.68239$ Å. The images were processed by using the CrysAlisPro software,[36] and the data were corrected for absorption by using the multiscan semiempirical method implemented in SADABS.[37] The structure was solved by using direct methods implemented in SHELXS-97[38,39] and refined from successive full-matrix least-squares cycles on F^2 by using SHELXL-97.[38,40] The non-hydrogen atoms were successfully refined by using anisotropic displacement parameters and the hydrogen bonds to carbon and oxygen atoms were located at their idealized positions by using the appropriate HFIX instructions in SHELXL: 43 for the aromatic carbon atoms, 13 for the CH group, 23 for the CH_2 carbon atoms, 137 for the terminal CH_3 methyl groups, and 147 for the hydroxy groups. All these atoms were included in subsequent refinement cycles in the riding-motion approximation with isotropic thermal displacements parameters (U_{iso}) fixed at 1.2 or $1.5\times U_{eq}$ of the relative atom.

Crystallographic-data collection and structural-refinement information for **RosCat1**·Cl·$CHCl_3$: formula = $C_{144}H_{156}Cl_{16}N_{12}O_{16}$; M_r = 2878.01; crystal size = 0.05 × 0.01 × 0.01 mm^3, $T = 100(2)$ K; triclinic; space group = $P\bar{1}$; $a = 12.0778(10)$, $b = 16.6966(13)$, $c = 18.2987(13)$ Å; $\alpha = 77.287(7)$, $\beta = 73.617(7)$, $\gamma = 76.710(7)^\circ$; $V = 3397.5(5)$ Å^3; $Z = 1$; $\rho_{calcd} = 1.407$ g cm^{-3}; $\mu = 0.393$ mm^{-1}; 27317 reflections collected, 19303 independent reflections, $R_{int} = 0.0555$;

$R1 = 0.2130$, and $wR2 = 0.4604$ for data $I > 2\sigma(I)$; $R1 = 0.2377$ and $wR2 = 0.4865$ for all data.

CCDC 1402129 contain the supplementary crystallographic data for this paper. These data are provided free of charge by The Cambridge Crystallographic Data Centre.

Theoretical calculations

The geometry of the two conformers of the **RosCat1** and **RosCat2** ligands (Figure 5) were fully optimized by using the B3LYP[41] DFT functional and the dzvp basis set.[42] Vibration-frequency calculations within the harmonic approximation were performed on the optimized geometries by using the same DFT method. The solvent effects of water and dichloromethane were evaluated by using the polarizable continuum model (PCM)[43] on the geometries fully optimized in solution. The standard Gibbs free-energy values at 298.15 K of each energy-minimum structure were calculated by adding the thermal correction obtained from the vibration-frequency analysis to the DFT energy calculated both in vacuum and solution (see Table S1 in the Supporting Information). Their lowest-energy electronic transitions were calculated by using the time-dependent DFT method[44] with the same functional and basis set described above. The geometries of the Fe^{III} coordination complexes with **RosCat1** and **RosCat2** (metal/ligand stoichiometry = 1:3, overall charge = 0, and spin multiplicity = 6) were fully optimized by using the semiempirical PM6 method.[45] All the calculations were performed by using the Gaussian09 program package.[46]

Mass-spectrometric analysis

Samples were prepared by dissolving each compound in methanol (1 mg mL^{-1}) and adding a stoichiometric amount of iron(III) chloride for complex formation (Fe/L = 1:3). Analysis was carried out by using MALDI with DCTB as the matrix. The samples were mixed (1:1) with a solution of DCTB in acetonitrile/water (70:30; 5 mg mL^{-1}) and droplets (1 μL) were applied on the MALDI target plate. Spectra were subsequently acquired in a Bruker ultrafleXtreme mass spectrometer operated in the positive-ion reflector mode, using delayed extraction in the range *m/z* 200–3500 with approximately 1500 laser shots. Full MS spectra were externally calibrated with a peptide mixture according to the manufacturer's instructions. Collision-induced dissociation (CID) tandem mass spectra (TOF/TOF-MS) were acquired with argon as the collision gas. The spectrometer LIFT method was externally calibrated with the Bombesin peptide (*m/z* 1619.82) and the respective CID fragment ions as mass standards. The mass spectrometer was operated with the FlexControl 3.4 software and data treatment was performed by using the FlexAnalysis 3.4 software package.

Acknowledgements

This work received financial support from the European Union (FEDER funds through COMPETE) and National Funds (FCT, Fundação para a Ciência e Tecnologia) through projects NORTE-07-0162-FEDER-000048, NORTE-07-0124-FEDER-000066/67, UID/QUI/50006/2013 (LAQV/REQUIMTE), and UID/Multi/04378/2013 (UCIBIO/REQUIMTE). The NMR spectrometers are part of the National NMR Network and were purchased within the framework of the National Program for Scientific Re-equipment, contract REDE/1517/RMN/2005, with funds from POCI 2010 (FEDER) and FCT. The authors are greatly indebted to all financing sources. A.L. and C.Q. also thank FCT their grants (SFRH/BPD/85793/2012 and SFRH/BD/79702/2011, respectively).

Keywords: amides · coordination modes · iron · ligand design · mass spectrometry

[1] S. J. Dixon, B. R. Stockwell, *Nat. Chem. Biol.* **2013**, *10*, 9–17.
[2] T. Zhou, Y. Ma, X. Kong, R. C. Hider, *Dalton Trans.* **2012**, *41*, 6371–6389.
[3] S. K. Sahoo, D. Sharma, R. K. Bera, G. Crisponi, J. F. Callan, *Chem. Soc. Rev.* **2012**, *41*, 7195–7227.
[4] R. C. Hider, X. Kong, *Nat. Prod. Rep.* **2010**, *27*, 637–657.
[5] C. Ji, R. E. Juárez-Hernández, M. J. Miller, *Future Med. Chem.* **2012**, *4*, 297–313.
[6] B.-K. An, X. Wang, P. L. Burn, P. Meredith, *ChemPhysChem* **2010**, *11*, 3517–3521.
[7] A. Avdeef, S. R. Sofen, T. L. Bregante, K. N. Raymond, *J. Am. Chem. Soc.* **1978**, *100*, 5362–5370.
[8] C. Queirós, A. M. G. Silva, S. C. Lopes, G. Ivanova, P. Gameiro, M. Rangel, *Dyes Pigm.* **2012**, *93*, 1447–1455.
[9] C. Queirós, A. Leite, M. G. M. Couto, T. Moniz, L. Cunha-Silva, P. Gameiro, A. M. G. Silva, M. Rangel, *Dyes Pigm.* **2014**, *110*, 193–202.
[10] C. Queirós, A. Leite, A. M. G. Silva, P. Gameiro, B. de Castro, M. Rangel, *Polyhedron* **2015**, *87*, 1–7.
[11] V. R. Pattabiraman, J. W. Bode, *Nature* **2011**, *480*, 471–479.
[12] A. L. Shanzer, S. Lifson, *Pure Appl. Chem.* **1992**, *64*, 1421–1435.
[13] S. K. Sahoo, M. Baral, B. K. Kanungo, *J. Chem. Eng. Data* **2011**, *56*, 2849–2855.
[14] M. E. Cass, T. M. Garrett, K. N. Raymond, *J. Am. Chem. Soc.* **1989**, *111*, 1677–1682.
[15] S. M. Cohen, B. O'Sullivan, K. N. Raymond, *Inorg. Chem.* **2000**, *39*, 4339–4346.
[16] R. J. Abergel, J. A. Warner, D. K. Shuh, K. N. Raymond, *J. Am. Chem. Soc.* **2006**, *128*, 8920–8931.
[17] W. Curatolo, A. Bali, C. M. Gupta, *J. Pharm. Sci.* **1985**, *74*, 1255–1258.
[18] A. S. Prakash, W. A. Denny, L. P. Wakelin, *Chem.-Biol. Interact.* **1990**, *76*, 241–248.
[19] I. C. S. Cardoso, A. L. Amorim, C. Queirós, S. C. Lopes, P. Gameiro, B. de Castro, M. Rangel, A. M. G. Silva, *Eur. J. Org. Chem.* **2012**, *2012*, 5810–5817.
[20] V. M. Nurchi, T. Pivetta, J. I. Lachowicz, G. Crisponi, *J. Inorg. Biochem.* **2009**, *103*, 227–236.
[21] A. Herath, R. Dahl, N. D. P. Cosford, *Org. Lett.* **2009**, *11*, 2043.
[22] E. Evangelio, J. Hernando, I. Imaz, G. G. Bardají, R. Alibés, F. Busqué, D. Ruiz-Molina, *Chem. Eur. J.* **2008**, *14*, 9754–9763.
[23] F. Riedel, S. Spange, *J. Phys. Org. Chem.* **2012**, *25*, 1261–1268.
[24] S. Fery-Forgues, D. Lavabre, *J. Chem. Educ.* **1999**, *76*, 1260–1264.
[25] a) B. Mennucci, *J. Am. Chem. Soc.* **2002**, *124*, 1506–1515; b) J. Tomasi, R. Cammi, B. Mennucci, C. Cappelli, S. Corni, *Phys. Chem. Chem. Phys.* **2002**, *4*, 5697–5712.
[26] T. Moniz, A. Nunes, A. M. G. Silva, C. Queirós, G. Ivanova, M. S. Gomes, M. Rangel, *J. Inorg. Biochem.* **2013**, *121*, 156–166.
[27] a) T. D. Rae, P. J. Schmidt, R. A. Pufahl, V. C. Cullota, T. V. O'Halloran, *Science* **1999**, *284*, 805–808; b) H. Glickstein, R. B. El, M. Shvartsman, Z. I. Cabantchik, *Blood* **2005**, *106*, 3242–3450.
[28] J. Balla, T. Kiss, R. F. Jameson, *Inorg. Chem.* **1992**, *31*, 58–62.
[29] a) R. Senthilnithy, M. D. P. De Costa, H. D. Gunawardhana, *Luminescence* **2009**, *24*, 203–208; b) A. J. Clarke, N. Yamamoto, P. Jensen, T. W. Hambley, *Dalton Trans.* **2009**, 10787–10798.
[30] a) W. Luo, Y. M. Ma, P. J. Quinn, R. C. Hider, Z. D. Liu, *J. Pharm. Pharmacol.* **2004**, *56*, 529–536; b) Y. Ma, W. Luo, P. J. Quinn, Z. Liu, R. C. Hider, *J. Med. Chem.* **2004**, *47*, 6349–6362; c) Y. Ma, H. De Groot, Z. Liu, R. C. Hider, F. Petrat, *Biochem. J.* **2006**, *395*, 49–55; d) S. Fakih, M. Podinovskaia, X. Kong, H. L. Collins, U. E. Schaible, R. C. Hider, *J. Med. Chem.* **2008**, *51*, 4539–4552.
[31] a) C. R. Lohani, K.-H. Lee, *Sens. Actuators B* **2010**, *143*, 649–654; b) S. Smanmoo, W. Nasomphan, P. Tangboriboonrat, *Inorg. Chem. Commun.* **2011**, *14*, 351–354; c) J.-M. Liu, Q.-Y. Zheng, J.-L. Yang, C.-F. Chen, Z.-T. Huang, *Tetrahedron Lett.* **2002**, *43*, 9209–9212.

[32] J. R. Lakowicz in *Principles of Fluorescence Spectroscopy,* 3rd ed., Springer, Berlin, Heidelberg, **2006**.
[33] A. T. R. Williams, S. A. Winfield, J. N. Miller, *Analyst* **1983**, *108*, 1067 – 1071.
[34] K. G. Casey, E. L. Quitevis, *J. Phys. Chem.* **1988**, *92*, 6590 – 6594.
[35] T. Kottke, D. Stalke, *J. Appl. Crystallogr.* **1993**, *26*, 615 – 619.
[36] *CrysAlisPro Software Package*, Version 1.171, Xcalibur Single Crystal CCD Diffractometer, Oxford Diffraction ed. **2006**.
[37] G. M. Sheldrick, *SADABS v.2.01*, Bruker/Siemens Area Detector Absorption Correction Program ed., Bruker AXS, Madison, Wisconsin, USA, **1998**.
[38] G. Sheldrick, *Acta Crystallogr. Sect. A* **2008**, *64*, 112 – 122.
[39] G. M. Sheldrick, *SHELXS-97 Program for Crystal Structure Solution*, University of Göttingen Göttingen **1997**.
[40] G. M. Sheldrick, *SHELXS-97 Program for Crystal Structure Refinement*, University of Göttinger Göttinger **1997**.
[41] a) A. D. Becke, *J. Chem. Phys.* **1993**, *98*, 5648 – 5652; b) C. Lee, W. Yang, R. G. Parr, *Phys. Rev. B* **1988**, *37*, 785 – 789; c) P. J. Stephens, J. F. Devlin, C. F. Chabalowsky, M. J. Frisch, *J. Phys. Chem.* **1994**, *98*, 11623 – 11627.
[42] N. Godbout, D. R. Salahub, J. Andzelm, E. Wimmer, *Can. J. Chem.* **1992**, *70*, 560 – 571.
[43] a) J. Tomasi, B. Mennucci, R. Cammi, *Chem. Rev.* **2005**, *105*, 2999 – 3093; b) G. Scalmani, M. J. Frisch, *J. Chem. Phys.* **2010**, *132*, 114110.
[44] a) M. E. Casida, M. Huix-Rotllant, *Annu. Rev. Phys. Chem.* **2012**, *63*, 287 – 323; b) C. Adamo, D. Jacquemin, *Chem. Soc. Rev.* **2013**, *42*, 845 – 856.
[45] J. J. P. Stewart, *J. Mol. Model.* **2007**, *13*, 1173 – 1213.
[46] M. Frisch, G. Trucks, H. Schlegel, G. Scuseria, M. Robb, J. Cheeseman, G. Scalmani, V. Barone, B. Mennucci, G. Petersson, H. Nakatsuji, M. Caricato, X. Li, H. Hratchian, A. Izmaylov, J. Bloino, G. Zheng, J. Sonnenberg, M. Hada, M. Ehara, K. Toyota, R. Fukuda, J. Hasegawa, M. Ishida, T. Nakajima, Y. Honda, O. Kitao, H. Nakai, T. Vreven, J. Montgomery, J. Peralta, F. Ogliaro, M. Bearpark, J. Heyd, E. Brothers, K. Kudin, V. Staroverov, R. Kobayashi, J. Normand, K. Raghavachari, A. Rendell, J. Burant, S. Iyengar, J. Tomasi, M. Cossi, N. Rega, J. Millam, M. Klene, J. Knox, J. Cross, V. Bakken, C. Adamo, J. Jaramillo, R. Gomperts, R. Stratmann, O. Yazyev, A. Austin, R. Cammi, C. Pomelli, J. Ochterski, R. Martin, K. Morokuma, V. Zakrzewski, G. Voth, P. Salvador, J. Dannenberg, S. Dapprich, A. Daniels, Farkas, J. Foresman, J. Ortiz, J. Cioslowski, D. Fox, Gaussian 09, Revision A1, Gaussian Inc., Wallingford CT, **2009**.

Received: May 28, 2015
Published online on September 7, 2015